


Quasistatic rheology of soft cellular systems using the cellular Potts modelFrançois Villemot and Marc Durand^{*}*Université de Paris, CNRS, UMR 7057, Matière et Systèmes Complexes (MSC), F-75006 Paris, France* (Received 6 April 2021; revised 19 July 2021; accepted 20 October 2021; published 10 November 2021)

Soft cellular systems, such as foams or biological tissues, exhibit highly complex rheological properties, even in the quasistatic regime, that numerical modeling can help to apprehend. We present a numerical implementation of quasistatic strain within the widely used cellular Potts model (CPM). The accuracy of the method is tested by simulating the quasistatic strain of two-dimensional dry foams, both ordered and disordered. The implementation of quasistatic strain in CPM allows the investigation of sophisticated interplays between stress-strain relationship and structural changes that take place in cellular systems.

DOI: [10.1103/PhysRevE.104.055303](https://doi.org/10.1103/PhysRevE.104.055303)**I. INTRODUCTION**

Soft cellular systems, which encompass foams, emulsions and biological tissues, are constituted of highly deformable—yet almost incompressible—units (bubbles, drops, cells), interacting through attractive adhesive interactions and soft steric repulsions. Interface energy is key to the cohesion and the rigidity of these systems, sometimes constituted solely of fluids. Under small strains, they behave elastically. Above a yield value, plastic rearrangements (called T1 events) occur, conferring to these systems a complex rheological behavior [1]. The relationship between the macroscopic response and the microscopic details, such as packing fraction and structural disorder, is still the subject of intense research activity [2–4]. Even the simplest case of quasistatic regime—in which the structure is at mechanical equilibrium at every time—is far from being fully understood, in particular in the shear banding phenomenon, which consists of the concentration of shear strain in localized zones (bands) and then the coexistence of flowing and stationary regions in a sheared material [5]. Numerical tools have been proven to be extremely useful to investigate the relationship between microscopic details and the macroscopic mechanical response [6–10]. The cellular Potts model (CPM) is one of the standard numerical modelings of multicellular systems, with various applications ranging from foam coarsening to collective behaviors of biological cells. However, because of its lattice-based modeling technique, it has been rarely used to investigate mechanical properties of cellular systems, except for a few exceptions [11,12].

In this paper, we present a rigorous implementation of quasistatic strain within CPM, offering a versatile tool to investigate the interplay between mechanical properties and other processes at work in cellular systems, such as coarsening in foams, or cell division and cell death in biological tissues. The outline of the paper is as follows. In Sec. II we introduce the cellular Potts model and show how it can be conveniently extended to simulate cellular systems under quasistatic strain.

The method is compared with other existing approaches, and extension to higher strain rates is discussed. In Sec. III we test the proposed method by analyzing the shear strain of two-dimensional (2D) dry foams. For a regular hexagonal foam, the shear modulus we obtain numerically agrees with the corresponding theoretical expression [13,14]. Yield strain is also analyzed. For disordered foams, we study the effect of disorder on the affinity of the displacement field and the shear modulus magnitude, and we compare our results with those reported in the literature.

II. MODELING QUASISTATIC STRAIN WITH CPM**A. Cellular Potts model**

The cellular Potts model (CPM), also called the Glazier-Graner-Hogeweg model, is one of the most accepted models of a multicellular system. It is widely used for simulating cellular systems in various fields of physics or biology, such as coarsening and mechanics of foams [11,15], tissue morphogenesis [16], cell sorting [17], and collective cell motion in epithelial tissues [18,19]. The CPM is a lattice-based model in which each cell in the system is given a different label (cell ID), and each lattice site k has a value σ_k taken from the list of cell IDs. A given cell is then represented by the subset of lattice sites that have its cell ID. A cell type $\tau(\sigma)$ can also be defined for each cellular domain. The CPM makes no assumption on the shape or the connectivity of the cellular domains, these properties are direct consequences of the energy terms of the Hamiltonian \mathcal{H} . In particular, walls between adjacent cells are allowed to fluctuate, and T1 events happen spontaneously. The CPM Hamiltonian \mathcal{H} that characterizes 2D soft cellular systems reads [17] as follows:

$$\mathcal{H} = \sum_{\text{neighboring sites } (k, l)} J_{\tau, \tau'} (1 - \delta_{\sigma_k, \sigma_l}) + \frac{B}{2A_0} \sum_{\text{cells } i} (A_i - A_0)^2. \quad (1)$$

^{*}marc.durand@univ-paris-diderot.fr

The first sum in Eq. (1) is carried over neighboring sites $\langle k, l \rangle$ and represents the boundary energy: each pair of neighbors having unmatching indices determines a boundary and contributes to the boundary energy. Here, σ_k and σ_l are the site values of sites k and l , respectively. δ is the Kronecker delta symbol: $\delta_{m,n} = 1$ if $m = n$, and 0 otherwise. τ and τ' are abbreviations for $\tau(\sigma_k)$ and $\tau(\sigma_l)$. $J_{\tau,\tau'} (= J_{\tau',\tau})$ is the energy per unit contact length between cell types τ and τ' . The second sum in Eq. (1) represents the compressive energy of the cells. A_i is the area of cell i , and A_0 is the nominal area. A factor of 2 has been introduced in the denominator so that B can be identified with the effective 2D bulk modulus of a cell, $-d^2\mathcal{H}/dA_i^2$.

The state of the system is updated via a Monte Carlo algorithm. A lattice site is first selected randomly. A target label is then randomly selected amongst this site's neighboring labels, and the update is accepted or discarded following a Metropolis-like rule which preserves the connectivity of cellular domains [20]. The acceptance probability in this Monte Carlo scheme requires a temperature, which has to be chosen carefully. Setting the temperature to a small value is analogous to performing an energy minimization, which is the usual choice to study the structure of dry foams. Higher temperatures will induce fluctuations in the boundaries between adjacent bubbles. Further increase of the temperature leads to large topological rearrangements and is useful to model biological systems, the simulation temperature reflecting the cellular activity.

B. Adding quasistatic strain to CPM

A common way to introduce strain in numerical simulations is by changing the shape of the simulation box. After proper equilibration, static properties of the materials can be measured directly for any given strain. However, such a method cannot be used in lattice-based modeling techniques like CPM. Nevertheless, strain can be applied by adding appropriate terms in the Hamiltonian. This approach has been used by Jiang and Glazier to simulate foams submitted to a time-dependent shear rate [11]. In this study, shear is introduced by adding an energy contribution of the bubble boundaries, either in the bulk or in those in contact with the two edges of the sample only, so that updates that move the wall in the direction of the shear are more likely to be accepted. The energy term added to the Hamiltonian is actually an energy gradient and is kept constant throughout the simulation. In the Monte Carlo algorithm, an energy gradient is analogous to a stress, so that the simulations are actually performed by applying a constant stress to the foam. The same method has been used by Raufaste *et al.* to simulate a foam flow around an obstacle [12]. One great advantage of this method is that it does not require one to wait for mechanical equilibration before incrementing the wall displacements. However, this approach has also a few drawbacks. First, when the strain energy term is applied on every bubble boundary (bulk strain), it overdetermines the displacement field. The case of a regular hexagonal foam is illustrative in this respect: the method implies an affine deformation of the bubble boundaries, which is not compatible with the Plateau's laws that impose equal 120° at mechanical equilibrium [9]. The

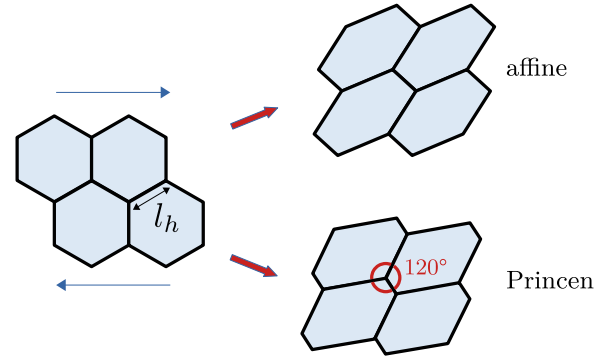


FIG. 1. Shape of deformed hexagonal bubbles following the affine displacement field (top right) and the Princen displacement field (bottom right). Only the latter satisfies the 120° joining angles that result from mechanical equilibrium.

exact deformation field which is compatible with the Plateau's has been derived by Princen [13,14] (see Sec. III B). Affine deformation and actual (Princen) deformation are compared in Fig. 1. As is discussed in Sec. III B, the shear modulus derived from affine deformation is 25% lower than the actual (Princen) shear modulus.

Similarly in Ref. [12], the added energy term sets the rheological behavior of the foam, resulting in a plug flow of the foam in the channel. Second, when the applied stress is larger than the yield value, the foam deformation produces a stress that opposes the one applied by the energy term. As a consequence, the actual shear rate of the simulation is not constant, but is the difference between the applied stress and the stress produced by the foam as an elastic response. This makes evaluating the actual shear strain quite difficult (in Ref. [11] it is assumed that it is proportional to the number of Monte Carlo steps).

We develop here an alternate method to simulate quasistatic strain within the CPM, while avoiding these drawbacks. It first requires the Potts lattice to be nonperiodic in one direction, which we choose to be the y direction. This nonperiodicity effectively creates a foam encased between two walls. To simulate a given strain created by the movement of these walls, we impose the displacement of the bubbles that touch the edges $y = \pm L/2$, where L is the size of the box in the y direction. This is done by adding the following term to the Hamiltonian:

$$\mathcal{H}_{\text{strain}} = \sum_i \frac{k}{2} \delta_{i,e} |\mathbf{r}_i - \mathbf{r}_i^*|^2, \quad (2)$$

where \mathbf{r}_i is the position of the center of mass (c.m.) of bubble i , and \mathbf{r}_i^* is its target position. For instance, to simulate a shear strain ϵ along the x direction, $\mathbf{r}_i^* = \epsilon y_i \mathbf{e}_x$, where \mathbf{e}_x is the unit vector along the x axis. The Kronecker $\delta_{i,e}$ in Eq. (2) is there to restrict the application of the strain to the bubbles in contact with the top and bottom edges of the box (symbolized with index e). The displacement and deformation of the bubbles in the bulk result only from the minimization of the total energy.

The constant k acts as a spring coefficient. Higher values will impose a stronger restraint on the position of the c.m. This value must be high enough so that the c.m. of each bubble stays in the vicinity of its target position, but not so high that it

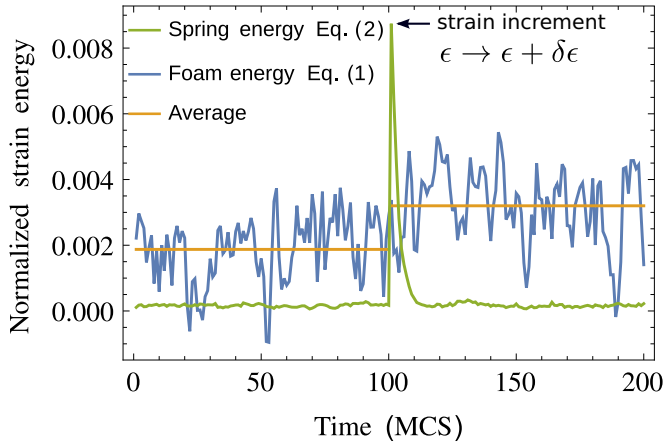


FIG. 2. Energy evolution during an increment of strain. Green curve: Spring energy [Eq. (2)] normalized by the foam energy at zero strain \mathcal{E}_0 . Blue curve: Foam energy \mathcal{E} [Eq. (1)] -1 normalized by \mathcal{E}_0 . Orange curve: Normalized foam energy averaged over time between two strain increments.

affects the shape of the bubbles. It can be chosen empirically: starting from a low value, the constant k can be increased until the average position of each c.m. is close enough to its target value (typically within a distance of 1 pixel). Alternatively, an estimation of a proper value can be obtained by considering the stress that these harmonic restraints apply on the bubbles. They create a potential energy gradient around the c.m. of bubble i , which is equivalent to a force of $k(\mathbf{r}_i - \mathbf{r}_i^*)$. This force is actually the shear stress that is applied to the system in order to induce the shear strain. In the elastic regime, this stress is proportional to the strain and depends only on the shear modulus. With an estimation of the shear modulus, we can find the value of k that will induce an average distance between the c.m. and its target position of any arbitrary value, typically chosen to be of the order of a pixel. With this method, k will depend linearly on the imposed shear strain.

The methodology to simulate quasistatic strain is then the following. Starting from an unstrained foam, we slowly increase the applied strain ϵ over multiple simulations. The strain is kept constant over the course of a given simulation, and the final configuration is used as the starting point of the simulation at a higher strain. The increments of ϵ must remain small in comparison with ℓ/L (where ℓ is the typical size of a bubble), especially at yield strain and above, to ensure that the structure relaxes in accordance with a true quasistatic regime; i.e., the succession of T1 events that would occur in a real foam is reproduced accurately. When ϵ is incremented, bubbles at the boundary translate to their final positions over the course of just a few Monte Carlo steps. However, proper equilibration over the whole sample takes longer and depends on both the temperature and the system size. We check that equilibrium is reached by monitoring the total energy, and we run each simulation until the energy fluctuates around a steady value. As an illustration, Fig. 2 shows the evolution of foam energy [Eq. (1)] and spring energy [Eq. (2)] during an increment of strain.

Ensemble averages and relevant quantities can be obtained for each value of the strain. In particular, the energy is used to

extract the relevant information about the elastic modulus and the yield strain. In the elastic regime, the stress is proportional to the strain, so that the strain energy varies quadratically with the strain, with a prefactor that depends only on the size of the system and the effective elastic modulus. For instance, the energy of a 2D medium with surface area \mathcal{A} under a shear strain ϵ is

$$\mathcal{E}(\epsilon) - \mathcal{E}_0 = \mathcal{A} \frac{G}{2} \epsilon^2, \quad (3)$$

where \mathcal{E}_0 is the energy at zero strain, and G is the 2D shear modulus. Yield strain is determined either by tracking the drop of the strain energy or counting the frequency of T1 rearrangements.

C. Validity beyond quasistatic regime

In the quasistatic regime, viscous dissipation plays no role, and the typical timescale of T1 rearrangements [21] is much smaller than the timescale of strain. Although it is tempting to simulate mechanics of cellular systems beyond the quasistatic regime, it must be warned that the CPM is a Monte Carlo simulation technique, and as such the kinetics of the relaxation process is determined by the Monte Carlo updating rule. Therefore, the rheological behavior in this regime will depend on the chosen updating rule. The CPM traditionally uses a Metropolis-like algorithm, because of its ability to mimic overdamped force-velocity behavior [22].

III. QUASISTATIC SHEAR OF 2D FOAMS

A. Initial state preparation

We test our method and assess its performances by simulating 2D foams under quasistatic shear strain. Although liquid content can be readily incorporated in the CPM, we assume the dry foam limit in this study. We first simulate regular hexagonal foams, for which quasistatic shear deformation, shear modulus, and yield strain can be calculated analytically. We then extend our study to polydisperse disordered foams, to check that our method allows us to capture the effect of disorder, and compare our results with those obtained in a previous study [7] using SURFACE EVOLVER, another popular numerical model for cellular systems [23].

For the regular hexagons, we use 100 bubbles on a 10×10 arrangement. Periodic boundaries are used along the x direction, but not along the y direction, which effectively results in walls at the top and bottom of the simulation box. The initial and target surface areas of the bubbles that lie at the boundaries are set to half of the surface area $A_0 = 1000 \text{ pixels}^2$ of the other bubbles. This is done so that interbubble edges meet with the boundaries at 90° angles, which is expected for a foam at rest. Special care is taken so that the aspect ratio of the simulation box matches the aspect ratio of a regular hexagonal lattice ($2/\sqrt{3}$).

The polydisperse foam is created from a random distribution of points in a square box. A Voronoi tessellation is done on this array of points to generate the starting configuration. Each bubble is given a random target surface area, A_0 , following a normal distribution with an average of 1000 pixels^2 and a standard deviation of $\Delta A = 125 \text{ pixels}^2$. The foam is then

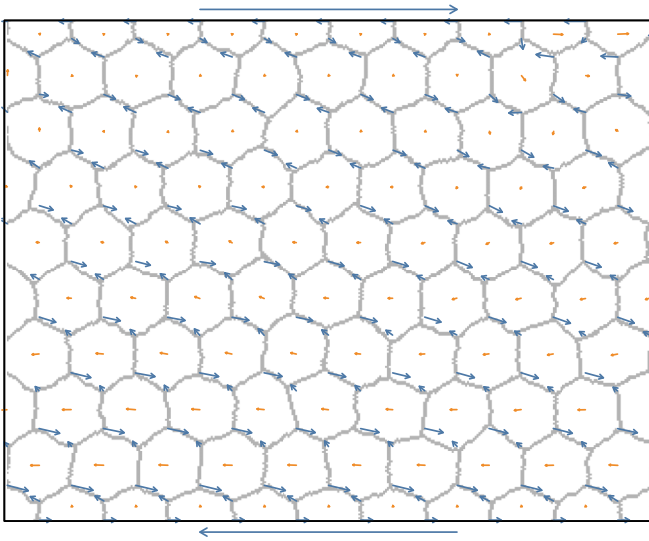


FIG. 3. Nonaffine component of the displacement field of the bubble centers (in red) and threefold junctions between edges (in blue) for a regular hexagonal foam under quasistatic shear (image corresponds to the strain value $\epsilon = 0.45$).

equilibrated in consecutive stages. A temperature annealing is first performed with a small bulk modulus B . Lowering the bulk modulus enhances topological rearrangements, resulting in faster and more thorough equilibration. In a second stage, the bulk modulus is progressively increased to a more realistic value. Finally, the foam is sheared along the x axis in both directions up to a strain of 0.1. This final step ensures that the shear loading that will be performed in the following will not trigger many, if any, T1 events. At the end of this equilibration procedure, the standard deviation of the distribution of side numbers per bubble is found to be $\Delta n = 0.48$.

In all our simulations, we set $J = 1$ and $B = 30$. Note that, as shearing is done at constant volume, the results are not really affected by the compressibility of the cells.

B. Hexagonal foam

1. Displacement field and shear modulus

For a regular, hexagonal foam, the deformation, and subsequently the elastic moduli, can be calculated analytically [13,14]: since the foam cells are spatially periodic, for any deformation, the centers of the hexagonal cells move affinely with the bulk. Cell symmetry implies that the midpoints of each edge also move affinely. Further, in any deformation, the edges remain planar, in accordance with Young and Laplace's equations. Note that, as a consequence, the threefold junctions between edges do not move affinely. We define the nonaffine component of the displacement field as the actual displacement field to which the affine displacement field ϵy is subtracted. Figure 3 shows the nonaffine displacement field of both the bubble centers and the edge junctions that we obtained numerically. In agreement with the theory, only bubble centers follow the affine displacement field.

The exact stress-strain relationship has been calculated by Princen, yielding the following expression for the shear

modulus [13,14]:

$$G_{\text{Princen}} = \frac{2\lambda}{\sqrt{3}l_h} \frac{1}{\sqrt{\epsilon^2 + 4}}, \quad (4)$$

where λ is the line tension (so an edge of length ℓ has an energy of $2\lambda\ell$) and l_h is the length of the side of a hexagon. Equation (4) gives the shear modulus for a foam up to the yield point. For small strains, its expression simplifies to

$$G_{\text{Princen}} = \frac{\lambda}{\sqrt{3}l_h}. \quad (5)$$

We can compare this expression with the shear modulus that the foam would have if the strain field was affine everywhere (what is called *bulk strain* in Ref. [11]). Using simple geometry arguments, and assuming $\epsilon \ll 1$, the strain energy is $\mathcal{E}_{\text{affine}} = \mathcal{E}_0 + \mathcal{A}\sqrt{3}\lambda\epsilon^2/8l_h$. Using Eq. (3), the associated shear modulus is then $G_{\text{affine}} = 3G_{\text{Princen}}/4$. Note that in CPM simulations, the line tension λ is proportional to J : $\lambda = zJ$, where the prefactor z depends on the range of interactions between lattice sites [24,25]. Actually, the underlying lattice introduces some anisotropy, so that z depends slightly on the orientation of the edge. Increasing the neighbor order helps to smooth out this anisotropy, but increases the computational cost. For this reason, we use fourth-neighbor order (corresponding to 20 neighbors per pixel) in our simulations, which is a good compromise between cost and accuracy. However, a residual anisotropy can still have significant impact on the mechanical response of the simulated foam, as edges tend to be pinned in orientations that minimize energy. This is especially pronounced for the regular hexagonal foam, whose edges have three possible orientations only. For disordered foams, anisotropy of the line tension is somehow smoothed out by the wider orientational distribution of the edges.

Fortunately, the effect of lattice anisotropy can be circumvented by increasing the simulation temperature, which has for effect to induce sampling over more edge orientations. However, increasing the temperature also tends to increase the overall energy of the system, mostly because the fluctuating edges are longer than at zero temperature. Precisely, when fluctuations are small, the increase in length of an edge at temperature T is proportional to its length at zero temperature: $\delta\ell = \ell T/2\lambda a$, where a ($a \sim 1$ pixel) is some cutoff length [25]. Therefore, one must evaluate G at different temperature values and then extrapolate its value at zero temperature to circumvent anisotropy artifacts.

For a given simulation temperature, a series of simulations is performed at different shear strains. A quadratic fit of $\mathcal{E} = f(\epsilon)$ gives us the numerical value of the shear modulus of the hexagonal foam G_{hex} . The value of G_{hex} as a function of the normalized temperature is reported in Fig. 4. For temperatures $T/J \leq 1.5$, the energy does not vary quadratically with the strain, because of the anisotropy of the underlying lattice, leading to inaccurate values of G_{hex} . For the temperature range $T/J > 1.5$ on the other hand, the quadratic fit converges and the reported value G_{hex} varies linearly with the simulation temperature. We adjust the value of the prefactor z such that the intercept of the linear fit of G_{hex} is equal to the theoretical value G_{Princen} [Eq. (5)]. We obtain $z = 10.50 \pm 0.07$, in very good agreement with other values reported in the literature [24–27] and, hence, confirming the accuracy of the method.

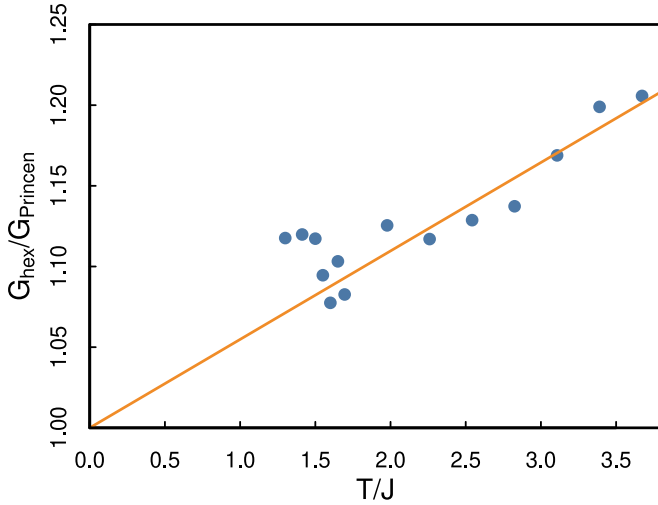


FIG. 4. Dimensionless shear modulus $G_{\text{hex}}/G_{\text{Princen}}$ of a hexagonal foam as a function of the normalized temperature T/J . The orange line represents the linear fit over the range $T/J > 1.5$.

2. Yield strain

Unlike shear modulus, the yield strain of a regular hexagonal foam changes with the orientation of the strain. With our chosen orientation (Fig. 3), the expected value is $2/\sqrt{3}$ [13,14]. Note that this theoretical value assumes that the foam is homogeneous and invariant by translation in both directions, so that at yield strain TIs occur simultaneously and uniformly in the hexagonal foam [13,14].

As for the shear modulus, we study the evolution of the yield strain with temperature and extrapolate to zero temperature to circumvent any effect of the underlying lattice anisotropy (Fig. 5). For a given temperature, the yield strain is determined by tracking the strain energy of the system: it is defined as the strain value at which energy drops abruptly, as illustrated in Fig. 6. Extrapolation leads to a yield strain value of 0.74 at zero temperature, which is significantly lower than the theoretical value. The cause of this discrepancy is the presence of the walls: in our simulations, as well as in real foams, the presence of these walls breaks the translational

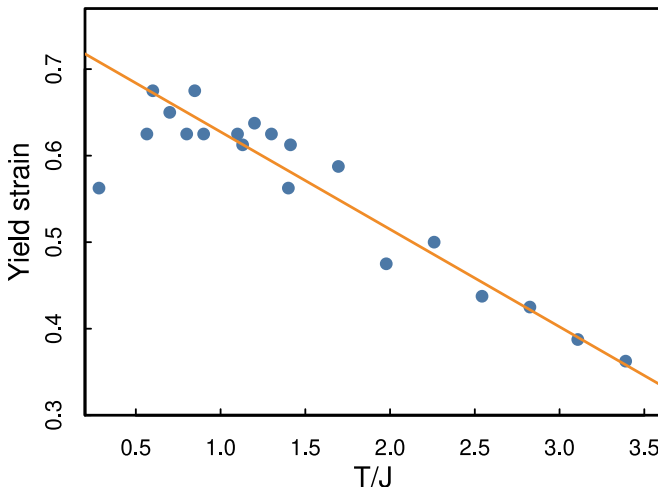


FIG. 5. Yield strain as a function of the normalized temperature.

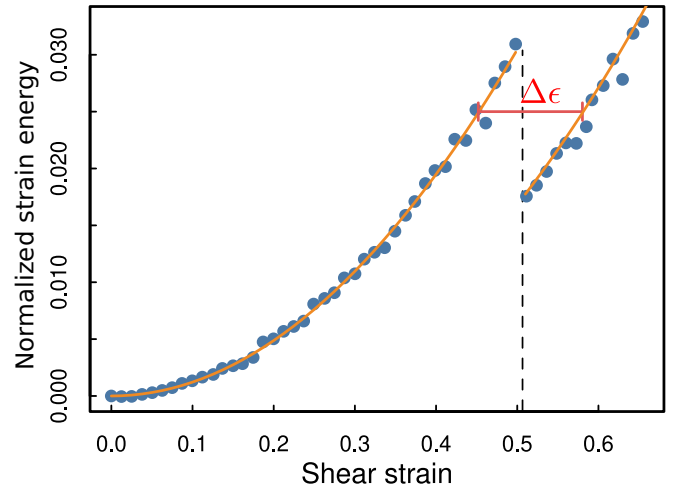


FIG. 6. Normalized strain energy $\mathcal{E}(\epsilon)/\mathcal{E}_0 - 1$ of a hexagonal foam as a function of the shear strain ϵ [Eq. (3)]. The yield strain is indicated by the dashed vertical line. The first orange curve is a quadratic fit of the simulation points below the yield strain of 0.51. The second curve is identical but offset to the right by a quantity of $\Delta\epsilon = 2/9\sqrt{3}$.

invariance in the y direction, because edges meet the walls at right angles [9]. As a consequence, edges in the vicinity of the walls are smaller than in the bulk, as this can be seen in Fig. 7, and the structure then relaxes through a line of TIs in the vicinity of one of the two walls at a strain lower than the theoretical yield value.

Because our system is periodic in the x direction, a shear band does not create any topological defect, it just changes the neighboring of the bubbles that belong to the two rows that slide with respect to each other. Therefore, the configuration right after the shear banding is still a hexagonal foam, but with a lower effective strain. This strain is actually lowered by a fixed amount: for a system of N rows of bubbles, a translation of one bubble to the side changes the strain by an amount of $\Delta\epsilon = 2/N\sqrt{3}$. Figure 6 shows the normalized strain energy as a function of the shear strain, for a normalized temperature of $T/J = 2.26$. The first curve on the graph is a quadratic fit of the simulation points below the yield strain of 0.51. The second curve corresponds to the same parabola, but offset to the right by a quantity of $\Delta\epsilon = 2/9\sqrt{3}$ (our simulation box

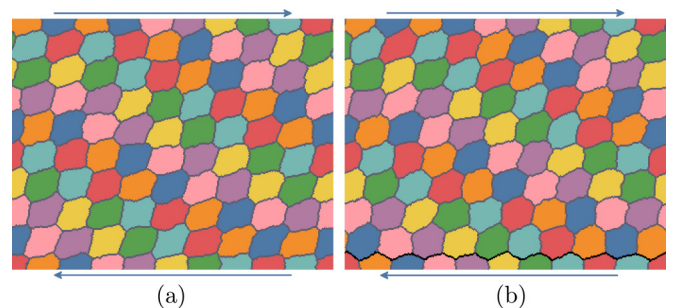


FIG. 7. Configurations right before and after the creation of a shear band. The black line indicates the localization of the shear band.

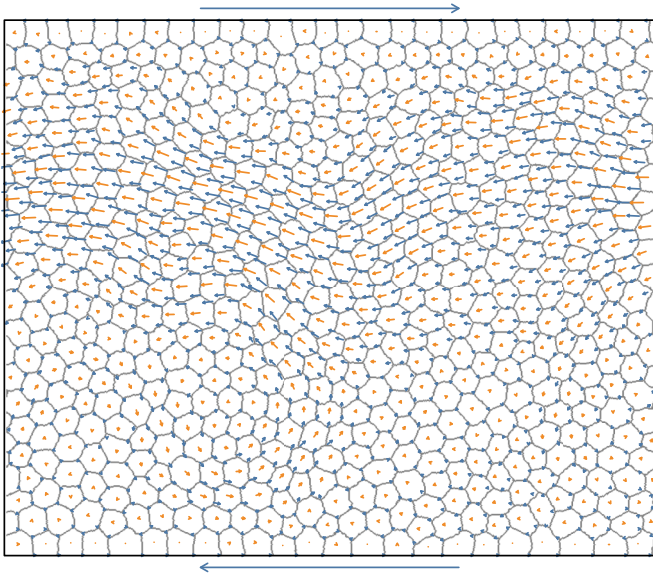


FIG. 8. Nonaffine component of the displacement field of the bubble centers (in red) and threefold junctions between edges (in blue) for the polydisperse foam under quasistatic shear (image corresponds to a strain value of $\epsilon = 0.10$).

contains ten rows, two of which are half rows). This second curve has no fitting parameter and shows that after a shear band the system still has the same shear modulus.

C. Polydisperse foam

We now test our method with a polydisperse, disordered foam. Structural disorder is known to affect the mechanical properties of foams [7,28], so it is important to check that our method allows one to detect the effect of structural disorder on the mechanical response of a 2D foam. As for the monodisperse case, we first plot the nonaffine component of the displacement field (see Fig. 8). In contrast with the regular case, both the bubble centers and the threefold edge junctions have a strong nonaffine component.

For the polydisperse foam, shearing was this time done along both $+x$ and $-x$ directions, as shown on Fig. 9. This setup improves the accuracy of the quadratic fit used to obtain the shear modulus and allows us to check that there is no residual stress in the initial state.

Once again, the shear modulus is measured at different temperatures, and then its zero temperature value is extrapolated from a linear fit. For each temperature, the temperature-dependent modulus G_{poly} was obtained from a quadratic fit of the energy. This modulus was then divided by the shear modulus of the hexagonal foam G_{hex} at the same temperature and with the same mean bubble area ($A_0 = 1000$ pixels²). Note that the ratio $G_{\text{poly}}/G_{\text{hex}}$ is then independent of z . Figure 10 shows that this normalized modulus converges to a constant value as temperature is increased. This plateau value is $\sim 89\%$ of the value found for perfect hexagons in our simulation. This value is consistent with those obtained by Cox and Whittick [7] with the SURFACE EVOLVER program [23], for foams with similar values of $\Delta A/\langle A \rangle$ and $\Delta n/\langle n \rangle$.

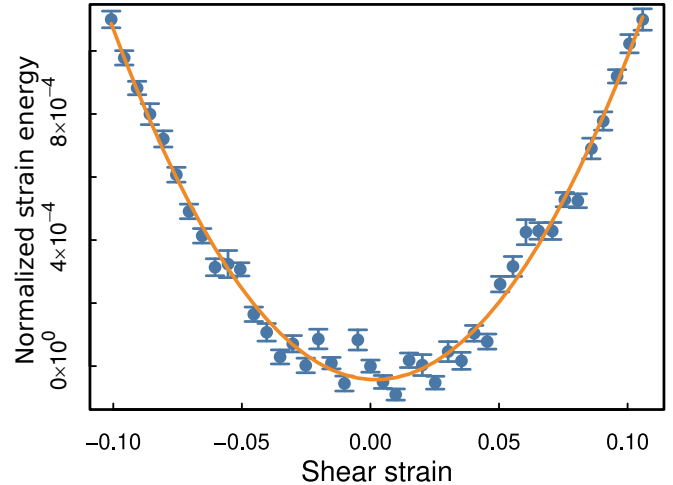


FIG. 9. Normalized strain energy $\mathcal{E}(\epsilon)/\mathcal{E}_0 - 1$ of a polydisperse foam as a function of the shear strain ϵ [Eq. (3)]. The orange curve is a quadratic fit.

IV. CONCLUSION

Numerical simulations are valuable tools to investigate the relationship between the mechanical response and the microscopic details of a cellular material, such as a foam or a biological tissue. The cellular Potts model is a standard numerical modeling tool of multicellular systems, with various applications ranging from foam coarsening to collective behaviors of biological cells. We have shown that quasistatic strain can easily be implemented in the CPM, and we have checked the accuracy of our method by analyzing the shear strain of 2D foams. For ordered foams, the shear modulus obtained numerically agrees well with the theoretical expression, and bubble centers follow affine displacement as expected. For disordered foams, bubble centers do not follow affine displacement and the shear modulus is found to be lower than for ordered foam with the same average bubble area. We obtained

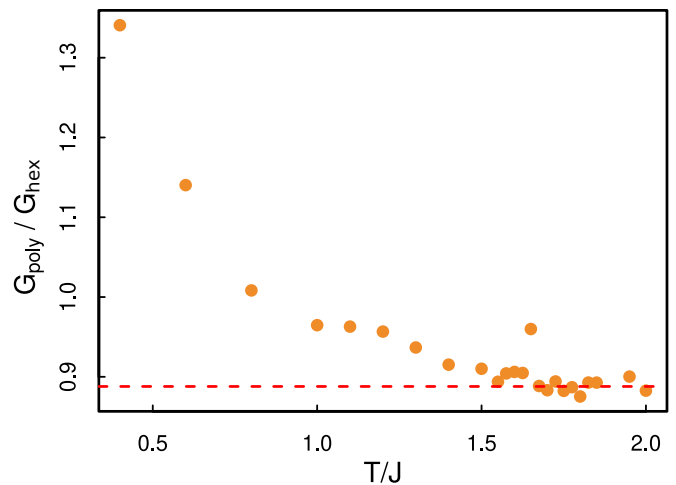


FIG. 10. Shear modulus of the polydisperse foam, normalized by the shear modulus of regular hexagonal foam with the same mean bubble area and at the same temperature, as a function of the normalized temperature T/J . The dashed red line represents the average value from simulations with $T/J > 1.5$.

good agreement with SURFACE EVOLVER simulations, another popular numerical model of multicellular systems. Systematic characterization of the effect of disorder will be investigated in a future study. More generally, the implementation of quasistatic strain into the CPM provides a versatile numerical tool to investigate the interplay between the rheological behavior and the additional structural changes that take place in cellular systems.

ACKNOWLEDGMENTS

ANR (Agence Nationale de la Recherche) and CGI (Commissariat à l'Investissement d'Avenir) are gratefully acknowledged for their financial support of this work through Labex SEAM (Science and Engineering for Advanced Materials and Devices), Grants No. ANR-11-LABX-086 and No. ANR-11-IDEX-0005-02.

-
- [1] S. Tlili, C. Gay, F. Graner, P. Marcq, F. Molino, and P. Saramito, *Eur. Phys. J. E* **38**, 33 (2015).
 - [2] D. Weaire, *Curr. Opin. Colloid Interface Sci.* **13**, 171 (2008).
 - [3] B. Dollet and C. Raufaste, *C. R. Phys.* **15**, 731 (2014).
 - [4] J.-C. G eminard, J. C. Pastenes, and F. Melo, *Phys. Rev. E* **97**, 042601 (2018).
 - [5] T. Divoux, M. A. Fardin, S. Manneville, and S. Lerouge, *Annu. Rev. Fluid Mech.* **48**, 81 (2016).
 - [6] A. Kabla and G. Debr egeas, *Phys. Rev. Lett.* **90**, 258303 (2003).
 - [7] S. J. Cox and E. L. Whittick, *Eur. Phys. J. E* **21**, 49 (2006).
 - [8] P. Guyot, A. M. Kraynik, D. Reinelt, and S. Cohen-Addad, *Soft Matter* **15**, 8227 (2019).
 - [9] I. Cantat, S. Cohen-Addad, F. Elias, R. H ohler, O. Pitois, F. Rouyer, and A. Saint-Jalmes, *Foams: Structure and Dynamics* (Oxford University, Oxford, 2018).
 - [10] J. M. Osborne, A. G. Fletcher, J. M. Pitt-Francis, P. K. Maini, and D. J. Gavaghan, *PLoS Comput. Biol.* **13**, e1005387 (2017).
 - [11] Y. Jiang, P. J. Swart, A. Saxena, M. Asipauskas, and J. A. Glazier, *Phys. Rev. E* **59**, 5819 (1999).
 - [12] C. Raufaste, B. Dollet, S. Cox, Y. Jiang, and F. Graner, *Eur. Phys. J. E* **23**, 217 (2007).
 - [13] H. M. Princen, *J. Colloid Interface Sci.* **91**, 160 (1983).
 - [14] S. A. Khan and R. C. Armstrong, *J. Non-Newtonian Fluid Mech.* **22**, 1 (1986).
 - [15] J. A. Glazier, M. P. Anderson, and G. S. Grest, *Philos. Mag. B* **62**, 615 (1990).
 - [16] T. Hirashima, E. G. Rens, and R. M. H. Merks, *Dev., Growth Differ.* **59**, 329 (2017).
 - [17] F. Graner and J. A. Glazier, *Phys. Rev. Lett.* **69**, 2013 (1992).
 - [18] A. Szab o, R.  unnep, E. M ehes, W. O. Twaal, W. S. Argraves, Y. Cao, and A. Czir ok, *Phys. Biol.* **7**, 046007 (2010).
 - [19] A. J. Kabla, *J. R. Soc., Interface* **9**, 3268 (2012).
 - [20] M. Durand and E. Guesnet, *Comput. Phys. Commun.* **208**, 54 (2016).
 - [21] M. Durand and H. A. Stone, *Phys. Rev. Lett.* **97**, 226101 (2006).
 - [22] J. A. Glazier, A. Balter, and N. J. Poplawski, in *Single-Cell-Based Models in Biology and Medicine*, edited by D. A. R. A. Anderson, P. M. A. J. Chaplain, and D. K. A. Rejniak, Mathematics and Biosciences in Interaction (Birkhauser, Basel, 2007), pp. 79–106.
 - [23] K. A. Brakke, *Experimental Mathematics* **1**, 141 (1992).
 - [24] R. Magno, V. A. Grieneisen, and A. F. Mar e, *BMC Biophys.* **8**, 8 (2015).
 - [25] F. Villemot, A. Calmettes, and M. Durand, *Soft Matter* **16**, 10358 (2020).
 - [26] J. K afer, T. Hayashi, A. F. Mar e, R. W. Carthew, and F. Graner, *Proc. Natl. Acad. Sci. U.S.A.* **104**, 18549 (2007).
 - [27] P. Marmottant, A. Mgharbel, J. K afer, B. Audren, J.-P. Rieu, J.-C. Vial, B. Van Der Sanden, A. F. Mar e, F. Graner, and H. Delano -Ayari, *Proc. Natl. Acad. Sci. U.S.A.* **106**, 17271 (2009).
 - [28] R. H ohler and S. Cohen-Addad, *J. Phys.: Condens. Matter* **17**, R1041 (2005).